RSC Advances




ROYAL SOCIETY OF CHEMISTRY

www.rsc.org/advances

Journal Name

RSCPublishing

ARTICLE

# Hydrothermal synthesis of $Li_4Ti_5O_{12}$ nanosheets as anode materials for lithium ion batteries

Cite this: DOI: 10.1039/xoxxoooooox

Hsin-Yi Wu [a], Min-Hsiung Hon [a, b], Chi-Yun Kuan [c] and Ing-Chi Leu [d, *]

Received ooth January 2015,
Accepted ooth January 2015

DOI: 10.1039/xoxxoooooox

www.rsc.org/

Spinel $Li_4Ti_5O_{12}$ (LTO) has the advantages of superior cycling performance, long and stable voltage plateau, enhanced safety, low cost, and environmental friendliness. LTO nanosheets were synthesized by a hydrothermal method using $Ti(OC_4H_9)_4$ and LiOH as the raw materials, followed by a subsequent heat treatment to get the desired phase. The effects of the reactant concentration and heat treatment temperature on the phase structure were studied to optimize process parameters for preparing the LTO nanosheets. The results demonstrate that the LTO nanosheets obtained by a hydrothermal method with 2 M LiOH and a followed heat treatment at 550°C exhibit an outstanding stable capacity of 175 mAh $g^{-1}$ at 0.1 C to 20 C for the 40 cycles. The ameliorated electrode-performance is ascribed to the nanostructure of the materials, which provides shorter diffusion-paths and a faster migration rate for both of ions and electrons. The newly synthesized nanostructure LTO materials can offer good high rate performance and stability. $Li_4Ti_5O_{12}$ nanosheets were developed in this paper for use as anode materials for lithium-ion power batteries with high-rate applications.

## Introduction

The development of high rate lithium ion batteries (LIBs) with high safety and long cycle life is essential for their use in some important fields, including fast charging electronics and electric vehicles [1, 2]. Conventional LIBs using graphite as the anode material generally suffer from poor performance in fast charge/discharge processes, along with significant serious safety problems [3, 4]. In contrast to the use of conventional graphite as an anode active material, $Li_4Ti_5O_{12}$ (LTO) can reduce the problem of lithium dendrites due to the lithium insertion/de-insertion, which occurs at a comparatively high voltage of about 1.55 V (vs. $Li/Li^+$). LTO has attracted attention as a promising anode material because of the near-zero change in the unit cell volume during charge and discharge processes [5-8]. LTO can accommodate lithium insertion during discharge, resulting in a structural transition from spinel-LTO to rock-salt phase $Li_7Ti_5O_{12}$ without noticeable changes in the lattice parameter. During cycling processes, lithium insertion into the spinel-LTO relocates lithium from tetrahedral 8a sites to the octahedral 16c sites with the formation of a rock-salt $Li_7Ti_5O_{12}$, which may be rendered as [9]

$$[Li]^{8a}[Li_{1/3}, Ti_{5/3}]^{16d}[O_4]^{32e} + e^- + \mathrm{Li}^+ = [Li_2]^{16c}[Li_{1/3}, Ti_{5/3}]^{16d}[O_4]^{32e}$$

These characteristics ensure a long life cycle and excellent cycle performance, making LTO an excellent candidate material for use in the power batteries of plug-in hybrid or full electric vehicles, which will be developed in the near future [10, 11]. The common synthesis methods of LTO, e.g., combustion synthesis [12], sol-gel [13-15], rheological phase reaction [16], molten-salt synthesis [17] and solid-state method [9, 18, 19], involve at least one high temperature step (over 900 °C) to obtain the crystalline LTO phase. Compared with the methods mentioned above, hydrothermal synthesis can decrease the activation energy for reaction, and LTO can be obtained at a lower temperature. In addition, various nanostructures of LTO, such as hollow microspheres [20], flower-like nanosheets [21], sawtooth-like nanosheets [22] and hierarchical structures [23] have been prepared using lithium hydroxide as the lithium source based on the hydrothermal method. Nevertheless, LTO suffers from a low intrinsic electronic conductivity and lithium-ion diffusion coefficient [24, 25], resulting in poor high-rate capacities. Extensive studies have been carried out to address these issues and different material modification schemes have been proposed with varied degree of success, including carbon coating [26, 27], metal and non-metal ion doping [25, 28], hybridization with carbon and metal powders [29-31], and reductions in LTO particle size [32].

After surveying the methods for preparing LTO reported in the literature, we found that it is not easy to directly prepare crystalline LTO, and that these methods usually require many processing steps and a high temperature environment. In this work, a simple hydrothermal synthesis process is employed to obtain LTO nanosheets with a large surface area. The results demonstrate that the synthesized LTO nanosheets had good cycling performance at high rates of 0.1 C to 20 C, thus making them a good choice for use in lithium ion batteries.

## Experimental

The LTO source used for preparing the nanosheets was commercially available tetrabutyl titanate ($Ti(OC_4H_9)_4$, Alfa Aesar). LTO nanosheets were hydrothermally synthesized from a mixture of $Ti(OC_4H_9)_4$ and lithium hydroxide (LiOH) in ethanol after vigorously stirring to form a sol. First, the $Ti(OC_4H_9)_4$ was added into the alcohol (99.8%). After stirring for 5 min, a transparent light yellow solution (named solution-A) was obtained. Second, the lithium hydroxide was added into the de-ionized water to form another solution (named solution-B). Finally, solutions A and B were mixed and stirred for 1 h to obtain a precursor solution, and then the mixture was transferred into a Teflon-lined stainless steel autoclave, sealed and maintained at 180 °C for 12 h. After the reaction, the sample was heat treated at 450 °C, 550 °C, 650 °C and 750 °C for 6h. Briefly, the hydrolysis reaction of $Ti(OC_4H_9)_4$ aqueous solution has been reported to form $TiO_2$:

$$(C_4H_9O)_4Ti + 4H_2O \leftrightarrow TiO_2 \cdot 2H_2O + 4C_4H_9OH \quad (1)$$

Lithium inserts into the $TiO_2$ can form mesophase lithium titanium oxide:

$$TiO_2 + 2LiOH \leftrightarrow Li_2TiO_3 + H_2O \quad (2)$$

Further reaction of mesophase lithium titanium oxide and $TiO_2$ can form the precursor of $Li_4Ti_5O_{12}$ phase:

$$Li_2TiO_3 + 4TiO_2 + 2LiOH \leftrightarrow Li_4Ti_5O_{12} + H_2O \quad (3)$$

The effects of different concentrations of LiOH on preparation of LTO nanosheets were studied. The prepared samples were characterized using powder X-ray diffraction (XRD, Rigaku Cu Kα, λ=1.54178 Å), field-emission scanning electron microscopy (FE-SEM, ZEISS AURIGA), transmission electron microscopy (TEM, JEOL JEM-2100F CS STEM) and Brunauer-Emmett-Teller surface area analysis (BET, Micromeritics ASAP 2010).

The working electrode was composed of an active material (LTO nanosheets), conductive agent (carbon black, super-P-Li), and water-based binder (PAA, poly-acrylic acid) in a weight ratio of 7:2:1. The mixture was then coated uniformly onto a copper foil. Lithium metal was used as the counter electrode. LiPF6 (1 M) in ethylene carbonate (EC) and diethyl carbonate (DEC) were used as the electrolyte (BASF Battery Materials Co., Ltd. ) at a volume ratio of 1:1. In order to examine the redox characteristics of the composite material anode in the lithium ion battery, the cells were galvanostatically charged and discharged over a voltage range of 0.8 V to 2.5 V vs. $Li/Li^+$ using a battery cycler (Arbin Inc., USA). In these tests, the applied charge/discharge potentials were in a range from 0.8 V to 2.5 V, the charge/discharge rates were set at 0.1 C, 0.5 C, 1 C, 2 C, 5 C, 10 C and 20 C (175 mAh $g^{-1}$, 1 C means insertion of 3 mol Li into $Li_4Ti_5O_{12}$ in 1 h), at room temperature. In order to examine the redox characteristics of the LTO anode in the lithium-ion battery, cyclic voltammetry was carried out using a potentiostat (EG&G Model 263A) at a scan rate of 0.05 mV $s^{-1}$ in a potential range of 0.8 V to 2.5 V.

## Results and discussion

XRD was performed on the as-prepared and heat-treated materials to examine the crystal structure. Figure 1 shows the XRD patterns of the as-prepared LTO anode nanomaterials obtained using the hydrothermal method and followed by heat treatment at various temperatures (pristine, 450°C, 550 °C, 650 °C and 750 °C, respectively). The sharp diffraction peaks in this figure show, that all the samples are well crystallized. Both the reactant concentration and synthesis temperature have a strong effect on the purity of the powders. When the concentration of the added LiOH was 2 M, the powders were mainly found to be spinel LTO; however small peaks of rutile $TiO_2$, anatase $TiO_2$ and $Li_2TiO_3$ were also observed at other concentrations (4M and 6M), implying an incomplete reaction. The results indicate that the Li/Ti molar ratio has a significant influence on the chemical composition of the final products. Single phase spinel LTO without any impurities was successfully prepared at 2 M LiOH for heat treatment at 450 °C, 550 °C, 650 °C and 750 °C. The morphologies of the products prepared in 2 M LiOH at different heat treatment temperatures are shown in Fig. 2. All the SEM images of the LTO samples are similar, and the LTO nanostructures appear as agglomerates assembled by many nanosheets. The results in Fig. 2a show the precursor LTO nanosheet synthesized by a hydrothermal process in LiOH solution at 180 °C for 12h. One can see that the samples are composed of very thin nanosheets. According to previous research [33], the development of this morphology is due to the growth of layered-structured titanates, such as $Li_xH_yTi_zO$, which form as intermediate products when titanium precursors are treated in LiOH by a hydrothermal process, and these can be converted to LTO nanosheets after heat treatment. This unique morphology enable the active material to come into contact with the electrolyte more effectively, as compared to other kinds of structures, thus improving the electrochemical properties. It is well known that a high surface area can provide more transport channels for lithium to insert into the electrode material, thus enhancing its capacity. Figure 2b~2e shows the SEM images of the precursor LTO after heat treatment. These clearly show that the products maintain the nanosheet structure after heat treatment. As the temperature increases, the heat-treated LTO nanosheets keep the original sheet-like morphology, although with an increased thickness compared to the precursor. However, the sintering of the precursor LTO nanosheets during heat treatment led to structural damage. The results also clearly indicate that heat treatment temperature significantly influences the thickness of nanosheets.

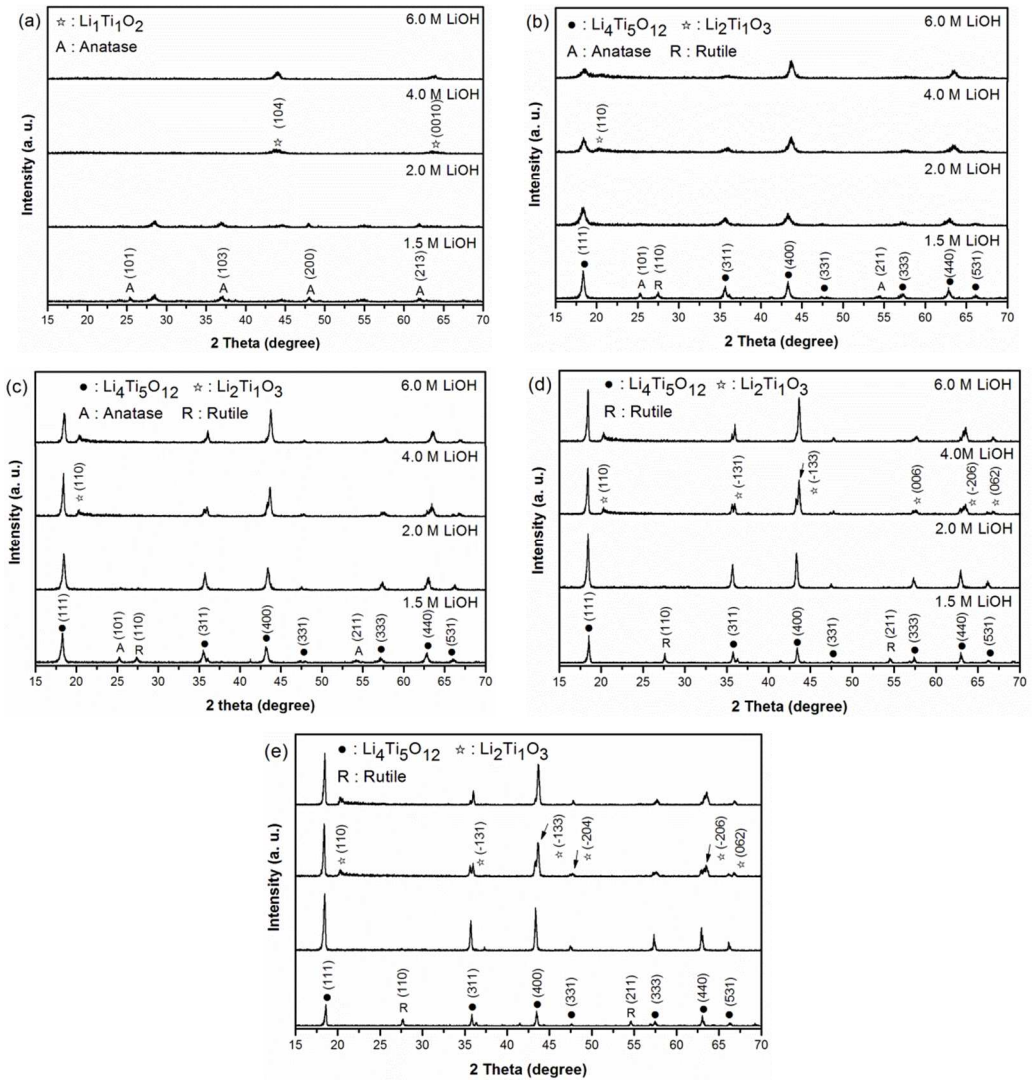


Fig. 1. X-ray diffraction patterns of LTO from reactants with different concentrations of LiOH (a) pristine and those that were subject to heat treatment in air at (b) 450 °C, (c) 550 °C, (d) 650 °C and (e) 750 °C.

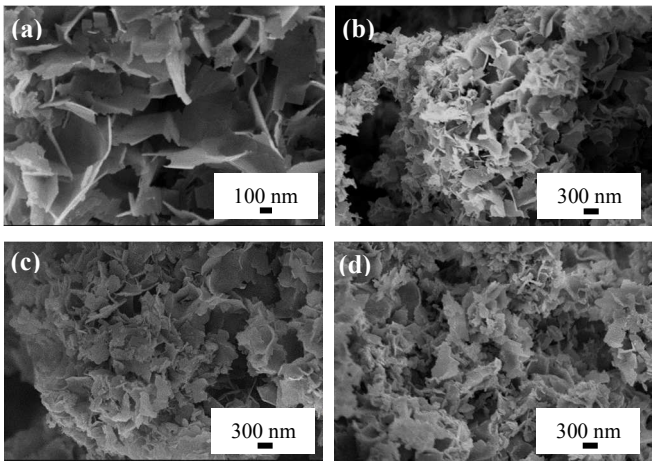


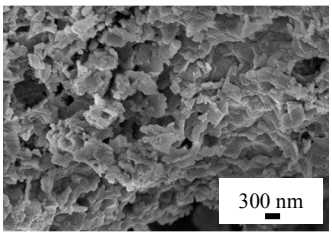


Fig. 2. SEM images of samples with different heat treatment temperatures using 2 M LiOH. (a) As-prepared, (b) 450 °C, (c) 550 °C, (d) 650 °C and (e) 750 °C.

Figure 3a shows HRTEM images of LTO nanosheets heat treated at 550 °C for 6 h, and it can be seen that the sample contained smaller sheets. The selected area electron diffraction (SAED) pattern in Fig. 3b also shows the (111), (311), (400) and (333) rings corresponding to the $Li_4Ti_5O_{12}$ phase. The assemblies of these sheets have a high BET surface area, and

specific surface areas for the pristine, 450 °C and 550 °C samples are 153.67 $m^2g^{-1}$, 93.88 $m^2$ $g^{-1}$ and 29.86 $m^2$ $g^{-1}$, respectively, which are still larger than those of $Li_4Ti_5O_{12}$ nanowires [34], nanotubes [35] and nanoflakes [36], though mush smaller after heat treatment. It is found that the isotherms show a typical type IV curve in the Fig. 4, which indicates a high surface area feature for the synthesized LTO samples.

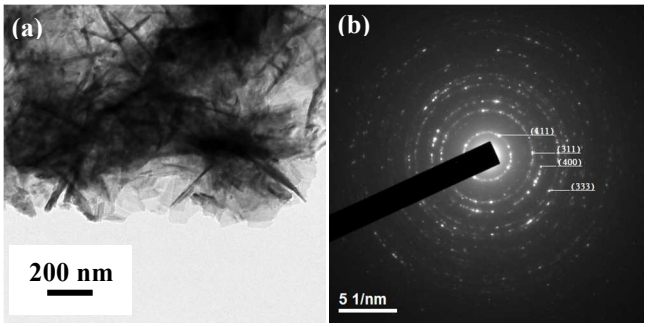


Fig. 3. (a) TEM images and (b) selected-area electron diffraction (SAED) patterns of $Li_4Ti_5O_{12}$ nanostructures using 2 M LiOH and heat treatment at 550 °C.

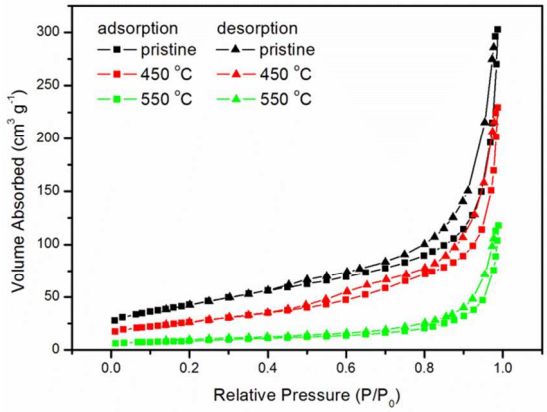


Fig. 4. Nitrogen adsorption-desorption isotherms for the samples calculated from the desorption isotherm using the Barrett-Joyner-Halenda (BJH) analysis method.

The electrochemical behaviour of the $Li_4Ti_5O_{12}$ electrode was investigated by CV and the results are shown in Fig. 5. The CV was performed to test the Li-intercalation in the LTO. The cathodic ($I < 0$) and anodic ($I > 0$) peaks indicate the insertion and extraction of lithium, respectively. The CV is typical for lithium intercalation in LTO. One pair of cathodic/anodic peaks [32] centered at 1.52/1.65 V and 1.50/1.69 V, corresponding to the lithium insertion/extraction in LTO at 450 °C and 550 °C, respectively. Figure 6 shows the rate capabilities of the samples. The cells were progressively charged/discharged in serial stages with the rate rising 0.1 C to 20 C. For each stage, the process was carried out in five cycles. According to Fig. 6a ~ 6c, although all stages showed good cyclability at different current rates, the rate capability depended significantly on the preparation temperature. There was a significant drop in capacity from the 2 C-rate, but the sample prepared at 450 °C showed sharp drop from the 5 C-rate. The discharge cycling performances of the $Li_4Ti_5O_{12}$ samples prepared at different heat treatment temperatures are shown in Fig. 6d. After 40 cycles at the different current rates of 0.1 to 20 C, the performances are stable for the LTO obtained with heat treatment at 550 °C. The 40-cycle discharge capacity can still be maintained at 175 mAh $g^{-1}$, and the curves show excellent performances with regard to the cycle stability, even at high current rate, which could be attributed to the small change in volume of the LTO during charge/discharge process. The initial capacity of the samples heat treated at 450 °C and 650 °C is exceed the theoretical capacitance, and this can be explained by the nanosheet structures of LTO having a faster lithium ion insertion process, short diffusion paths and the enhanced contact area between the LTO and electrolyte. It is interesting to note that the LTO nanostructures prepared in this study have capacities that are far better than the theoretical charge/discharge properties. This is because [32] the near-surface environment of the nanosized particles allows higher Li ion occupancies, leading to a larger storage capacity. The fact that smaller particle sizes lead to larger capacities suggests that the simultaneous 8a and 16c occupation is more easily accommodated in the near-surface region of the particles compared to the bulk, explaining the relatively high charge/discharge voltages at which it takes place. Besides, in a systematic particle size dependent study [37], Kavan et al. concluded that reducing the LTO particle size leads to a systematic decrease in the Li diffusion coefficient, compensated for by the large surface area, accounting for an optimal particle size using 2M LiOH for 550 °C depending on the charge/discharge rate. Another conventional viewpoint [38] states that the theoretical capacity of spinel $Li_4Ti_5O_{12}$ is limited by the number of available octahedral sites to accommodate lithium ions. In the intercalation process, additional lithium ions are added into the lattice and located at the octahedral (16c) sites. Because the amount of octahedral (16c) sites is twice that of the tetrahedral (8a) sites in $Li_4Ti_5O_{12}$, only 3 mol lithium ions can intercalate into $Li_4Ti_5O_{12}$ according to the classical viewpoint. However, there are still tetravalent titanium ions (40% of all titanium ions) in the reduction product of $Li_7Ti_5O_{12}$ that are able to accept ions. Accordingly, another 2 mol lithium ions could be intercalated into $Li_7Ti_5O_{12}$ if there are enough interstitial sites in $Li_7Ti_5O_{12}$. Lithium insertion in this kind of material is just like surface lithium storage, and this process can thus meet the requirement for fast lithium storage.

In this work, we use a simpler method to prepare the LTO nanosheets that can have a nanostructure with high specific surface area at a lower heat treatment temperature, as compared with other high temperature processes reported in the literature [39].

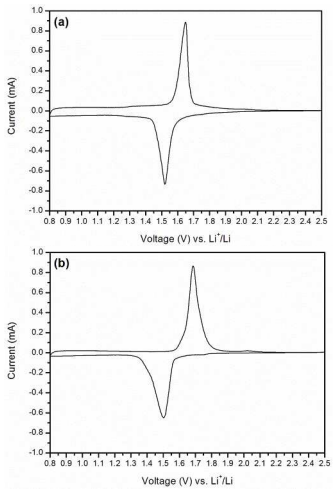


Fig. 5. CV profiles of $Li_4Ti_5O_{12}$ electrode at a scan rate of 0.5 mV $s^{-1}$ between 0.8 and 2.5 V. (a) 450 °C and (b) 550 °C.

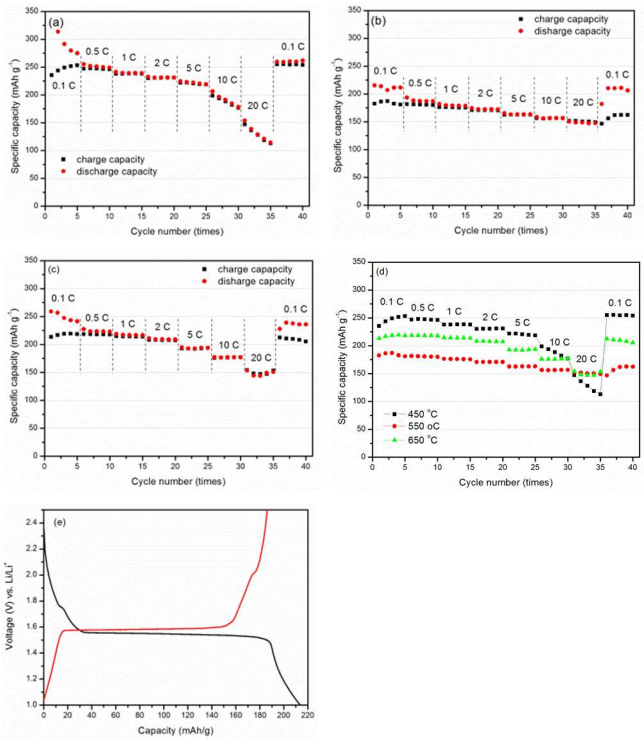


Fig. 6. Cycling performance curves of $Li_4Ti_5O_{12}$ synthesized at different heat treatment temperatures at 0.1 C, 0.2 C, 1 C, 2 C, 5 C, 10 C and 20 C rates. (a) 450 °C, (b) 550 °C, (c) 650 °C, (d) cyclic charging performance of all samples and (e) the electrodes of the 550 °C of first charge-discharge curves at 0.1 C rate.

## Conclusions

In summary, we have successfully synthesized spinel LTO nanosheets via a hydrothermal method and subsequent low temperature heat treatment, and use them as anode materials for a lithium ion battery. According to the XRD patterns, LTO were obtained by using 2 M LiOH aqueous solution and heat treated at 550 °C for 6 h. As a result of electrochemical characterization, the hydrothermal LTO nanosheets subjected to heat treatment at 550 °C can exhibit a good charge/discharge capacity of about 175 mAh $g^{-1}$ under different current rates when the cut-off voltage is from 0.8 to 2.5 V. The superior performance of the LTO nanosheets in LIBs is due to their high surface area as well as short Li ion diffusion paths, which help to retain a low level of polarization and a high degree of lithium ion insertion. From these results, it can be concluded that LTO can be prepared by low temperature processes and is a very promising material for use as an anode of LIBs.

## Acknowledgements

This study was supported by the Ministry of Science and Technology, Republic of China (MOST 100-2221-E-006-123-MY3 and NSC 102-2221-E-024-003-MY3), which is greatly appreciated.

## Notes and references

[a] Department of Materials Science and Engineering, National Cheng Kung University, Tainan, Taiwan, ROC.
[b] Research Center for Energy Technology and Strategy, National Cheng Kung University, Tainan, Taiwan, ROC.
[c] Technical Department, Thintech Materials Technology Co., LTD., Kaohsiung, Taiwan, ROC.
[d] Department of Materials Science, National University of Tainan, Tainan, Taiwan, ROC.
* Corresponding author: icleu@mail.mse.ncku.edu.tw (Ing-Chi Leu)

1. A. Manthiram, *J. Phys. Chem. Lett.*, 2011, **2**, 176.
2. M. Armand, J. M Tarascon, *Nature*, 2008, **451**, 652.
3. L. Ji, Z. Lin, M. Alcoutlabi, X. Zhang, *Energy Environ. Sci.*, 2011, **4**, 2682.
4. J. Jiang, Y. Li, J. Liu, X. Huang, C. Yuan, X. W. Lou, *Adv. Mater.*, 2012, **24**, 5166.
5. S. W. Han, J.H. Ryu, J. Jeong, D.H. Yoon, *J. Alloys Comp.*, 2013, **570**, 144.
6. A. S. Prakash, P. Manikandan, K. Ramesha, M. Sathiya, J.M. Tarascon, A.K. Shukla, *Chem. Mater.*, 2010, **22**, 2857.
7. X. F. Guo, C. Y. Wang, M. M. Chen, *Mater. Lett.*, 2012, **83**, 39.
8. C. Y. Lin, J. G. Duh, *J. Alloys Comp.*, 2011, **509**, 3682.
9. T. Ohzuku, A. Ueda, N. Yamamoto, J. Electrochem Soc, 1995, **142**, 1431.
10. Y. J. Lee, S. Y. Park, J. G. Seo, J. R. Yoon, J. H. Yi, I. K. Song, *Curr. Appl. Phys.*, 2011, **11**, 631.
11. T. Yuan, R. Cai, K. Wang, R. Ran, S. Liu, Zo. Shao, *Ceram. Int.*, 2009, **35**, 1757.
12. M. Venkateswarlu, C. H. Chen, J. S. Do, C. W. Lin, T. C. Chou, B. J. Hwang, *J. Power Sources*, 2005, **146**, 204.
13. J. Gao, C. Y. Jiang, J. R. Ying, C. R. Wan, *J. Power Sources*, 2006, **155**, 364.
14. Y. J. Hao, Q. Y. Lai, J. Z. Lu, H. L. Wang, Y. D. Chen, X. Y. Ji, *J. Power Sources*, 2006, **158**, 1358.

15. S. Y. Yin, L. Song, X. Y. Wang, M. F. Zhang, K. L. Zhang, Y. X. Zhang, *Electrochim. Acta*, 2009, **54**, 5629.
16. M. M. Rahman, J. Z. Wang, M. F. Hassan, S. Chou, D. Wexler, H. K. Liu, *J. Power Sources*, 2010, **195**, 4297.
17. T. Ohzuku, A. Ueda, N. Yamamoto, *J. Electrochem. Soc.*, 1995, **142**, 1431.
18. K. Zaghib, M. Armand, M. Gauthier, *J. Electrochem. Soc.*, 1998, **145**, 3135.
19. K. Zaghib, M. Simoneau, M. Armand, M. Gauthier, *J. Power Sources*, 1999, **81**, 300.
20. S. X. Deng, J. W. Li, S. B. Sun, H. Wang, J. B. Liu, H. Yan, *Electrochimica Acta*, 2014, **146**, 37.
21. Y. Tang, L. Yang, S. Fang, Z. Qiu, *Electrochim. Acta*, 2009, **54**, 6244.
22. Y. F. Tang, L. Yang, Z. Qiu, J. S. Huang, *Electrochem. Commun.*, 2008, **10**, 1513.
23. J. Chen, L. Yang, S. Fang, Y. Tang, *Electrochim. Acta*, 2010, **55**, 6596.
24. Y. Q. Wang, L. Gu, Y. G. Guo, H. Li, X. Q. He, S. Tsukimoto, Y. Ikuhara, L. J. Wan, *J. Am. Chem. Soc.*, 2012, **134**, 7874.
25. L. Zhao, Y. S. Hu, H. Li, Z. X. Wang, L. Q. Chen, *Adv. Mater.*, 2011, **23**, 1385.
26. B. Li, C. Han, Y. B. He, C. Yang, H. Du, Q. H. Yang, F. Kang, *Energy Environ. Sci.*, 2012, **5**, 9595.
27. H. G. Jung, S. T. Myung, C. S. Yoon, S. B. Son, K. H. Oh, K. Amine, B. Scrosati, Y. K. Sun, *Energy Environ. Sci.*, 2011, **4**, 1345.
28. K. S. Park, A. Benayad, D. J. Kang, S. G. Doo, *J. Am. Chem. Soc.*, 2008, **130**, 14930.
29. X. Li, M. Z. Qu, Y. J. Huai, Z. L. Yu, *Electrochim. Acta*, 2010, **55**, 2978.
30. R. Cai, X. Yu, X. Liu, Z. Shao, *J. Power Sources*, 2010, **195**, 8244.
31. B. Zhang, Y. Yu, Y. Liu, Z. D. Huang, Y. B. He, J. K. Kim, *Nanoscale*, 2013, **5**, 2100.
32. W. J. H. Borghols, M. Wagemaker, U. Lafont, E. M. Kelder, F. M. Mulder, *J. Am. Chem. Soc.*, 2009, **131**, 17786.
33. H. Y. Wu, M. H. Hon, C. Y. Kuan, I. C. Leu, *J. Electron. Mater.*, 2014, **43**, 1048.
34. L. Cheng, J. Yan, G. N. Zhu, J. Y. Luo, C.X. Wang, Y. Y. Xia, *J. Mater. Chem.*, 2010, **20**, 595.
35. J. Kim, J. Cho, Electrochem. *Solid State Lett.*, 2007, **10**, A81.
36. Y. M. Jiang, K. X. Wang, H. J. Zhang, J. F. Wang, J. S. Chen, *Sci Rep*, 2013, **3**, 3490.
37. H. Ge, N. Li, D. Li, C. Dai, D. Wang, *J. Phys. Chem. C*, 2009, **113**, 16.
38. T. F. Yi, Z. K. Fang, L. Deng, L. Wang, Y. Xie, Y. R. Zhu, J. H. Yao, C. Dai, *Ceram. Int.*, 2015, **41**, 2336.
39. J. Chen, L. Yang, S. Fang, Y. Tang, *Electrochimica Acta*, 2010, **55**, 6596.



 